frontiers | Frontiers in Sensors

TYPE Original Research
PUBLISHED 05 December 2024
DOI 10.3389/fsens.2024.1430958

Check for updates

OPEN ACCESS

EDITED BY
Laís Canniatti Brazaca,
São Paulo State University, Brazil

REVIEWED BY
Shofarul Wustoni,
King Abdullah University of Science and Technology, Saudi Arabia
Ajay Kumar,
Jaypee Institute of Information Technology, India

*CORRESPONDENCE
Manisha Gupta,
mgupta1@ualberta.ca

†These authors have contributed equally to this work

RECEIVED 10 May 2024
ACCEPTED 19 November 2024
PUBLISHED 05 December 2024

CITATION
Fan J, Kang S and Gupta M (2024) Long-term stability of N-heterocyclic carbene (NHC) functionalized organic electrochemical transistor (OECT) for biosensing applications. *Front. Sens.* 5:1430958.
doi: 10.3389/fsens.2024.1430958

COPYRIGHT
© 2024 Fan, Kang and Gupta. This is an open-access article distributed under the terms of the Creative Commons Attribution License (CC BY). The use, distribution or reproduction in other forums is permitted, provided the original author(s) and the copyright owner(s) are credited and that the original publication in this journal is cited, in accordance with accepted academic practice. No use, distribution or reproduction is permitted which does not comply with these terms.

Long-term stability of N-heterocyclic carbene (NHC) functionalized organic electrochemical transistor (OECT) for biosensing applications

Jiaxin Fan[1†], Seongdae Kang[2†] and Manisha Gupta[1*]

[1]Department of Electrical and Computer Engineering, University of Alberta, Edmonton, AB, Canada, [2]Department of Chemical and Material Engineering, University of Alberta, Edmonton, AB, Canada

The increasing demand for the rapid identification of various pathogens and disease biomarkers makes it essential to develop selective and reliable biosensors. The three basic components of a biosensor are: (i) the bioreceptor that binds to the target analyte, (ii) the transducer that converts the signal, and (iii) a signal processing circuit. Integrating the biorecognition elements onto the transducer surface is a critical step that governs the selectivity and reliability of biosensors. Here, we present a novel approach for functionalizing aerosol jet-printed organic electrochemical transistors (OECTs) for biosensing applications. Our design utilizes a printed Au gate modified with N-heterocyclic carbene (NHC) linkers for biofunctionalization. NHC was selected due to its excellent stability and high binding affinity with transition metals, facilitating a robust biofunctionalization mechanism. Utilizing the NHC-Au surfaces, we developed OECT-based biosensors that successfully detected the biotin-streptavidin (biotin-SA) binding events as threshold voltage shift (ΔV_T) of 193 $\pm$ 64 mV, which is approximately three-fold of that for bovine serum albumin (BSA) (62 $\pm$ 41 mV), indicating the NHC functionalized OECT-based biosensor is selective towards the target analyte. In addition, the NHC-Au electrode and the printed OECT both remained functional after 24 months of storage at room temperature, with comparable performances (ΔV_T = 161 $\pm$ 30 mV for SA binding) as the freshly prepared ones, demonstrating outstanding long-term stability. To the best of our knowledge, this is the first study combining NHC and OECT for biosensing and showcasing 24-month long-term stability. Given the versatility of NHCs in forming highly stable covalent bonds with most transition metals, this study is an important demonstration of their application in bioelectronics. Thus, we have shown a prominent biosensor development technology based on carbenes and organic electronics, which can be adapted to various biomolecule detection and biomedical applications. The exceptional stability of the printed OECTs and NHC functionalized gate highlights their potential for long-term biosensing applications, paving the way for reliable bioelectronics.

KEYWORDS

N-heterocyclic carbene, NHC, OECT, biosensor, aerosol jet printing, functionalization

1 Introduction

Organic electrochemical transistors (OECTs) have attracted a considerable amount of research attention during the past few decades for developing next-generation bioelectronics (Sophocleous et al., 2020; Shen et al., 2021), as they are compatible with aqueous environments with low operating voltages and capable of converting the ionic signal to an electrical one with intrinsic amplification. A variety of biological and chemical sensing has been achieved by altering the OECT materials and functionalizing device surfaces (Strakosas et al., 2014; Liao et al., 2019; Wang et al., 2019; Chen et al., 2021; Fan et al., 2021; Guo et al., 2021; Liu et al., 2021). Surface functionalization is essential to attain the desired selectivity and sensitivity. OECTs are three-terminal devices with source, drain, and gate contact, and a conducting polymer channel between the source and drain. As both the channel and the gate are immersed in an electrolyte and in contact with the analyte, surface modification has been mainly focused on the channel and the gate electrode. Functionalizing the channel provides a direct indication of the interaction with the analyte, but it may deteriorate the channel material and reduce the sensor performance (Fan et al., 2021). Gate functionalization offers the advantage of tailoring the interfacial properties without affecting the channel conductivity. Using an external gate electrode allows the functionalization process to be completely isolated from the rest of the device, facilitating more versatile functionalization approaches while retaining the device performance for high sensitivity.

Biosensor functionalization can be performed using physisorption and chemisorption. Even though physisorption is the simplest functionalization method, the functionalized surface is susceptible to changes in the storage temperature and pH, and physisorption may not be suitable for all types of biomolecules. For chemisorption techniques, strong covalent bonds are formed between the biomolecules and the transducer surface, and the orientation of attachment could also be controlled to obtain a more homogenous functionalized surface (Liebana and Drago, 2016; Zhang et al., 2020). Self-assembled monolayers (SAMs) of organic molecules are widely used to activate the sensor surface with functional groups to facilitate biomolecule attachment. Thiol-based ligands are the most common molecule class for functionalizing gold surfaces, which utilizes the interaction between sulfur and gold. Thiol-based functional groups have been widely implemented in biomolecule sensing technologies (Lim et al., 2014; Welch et al., 2017; Ataman Sadık et al., 2018; Gentili et al., 2018). However, the main challenges associated with thiol-based SAMs are their rapid oxidation and degradation under ambient conditions (Lee et al., 1998; Schoenfisch and Pemberton, 1998; Willey et al., 2005; Srisombat et al., 2011), limiting their application under ambient and aqueous environments, which are often required for biosensing applications. Therefore, developing an alternative functional group, which has excellent stability and is easy to be attached, is critical to boost the development of next-generation bioelectronics.

N-heterocyclic carbenes (NHCs), as strong σ-donors, are known to form strong bonds with gold and other transition metals; therefore, NHC-metal complexes have been extensively studied for homogeneous catalysis and metallopharmaceuticals (Hopkinson et al., 2014; Cerquera-Montealegre et al., 2024). NHC complexes have also been applied for carbon dioxide capturing and functionalizing (Stiernet et al., 2023; Fan et al., 2024). NHCs on gold nanoparticles and surfaces have shown great potential in various applications, ranging from biomedical to electronics (Kang et al., 2021; Kaur et al., 2022; Qiao et al., 2023). The C atom in NHC bonds to the surface metal atom via stronger covalent bonding as compared to the S atom in a typical thiol ligand (Kang et al., 2021). The Au-C bond in NHC has larger dissociation energy (67 kcal/mol) (Zhukhovitskiy et al., 2013) and short bond length (2.0 Å) (Zhukhovitskiy et al., 2013) as compared to a typical Au-S bond (45 kcal/mol (Nuzzo et al., 1987) and 2.2–2.6 Å (Jadzinsky et al., 2007)). Crudden et al. demonstrated ultra-stable NHC SAMs on Au surfaces. Once bound to the Au surface, NHC-based SAMs have shown high thermal, hydrolytic, chemical, oxidative, and electrochemical stabilities (Crudden et al., 2014), which are promising properties for biosensing applications. There have been several biosensors based on NHC-modified Au surfaces, and they are mainly based on optical sensing techniques, such as surface plasmon resonance (SPR) (Li et al., 2017; Li et al., 2018) and colorimetric detection (Zhang et al., 2023). Mayall et al. demonstrated an electrochemical biosensor based on NHC-modified Au for measles virus detection (Mayall et al., 2020). Bacteria detection was achieved by Singh et al. using a new electrochemical biosensor developed with NHC and toll-like receptor proteins (Singh et al., 2021). Recently, NHC-SAM was utilized for conjugating target-specific bioreceptors to graphene field-effect transistors for POC pathogen detection (Kim et al., 2024).

Here, we demonstrated biosensing using aerosol jet printed OECTs with Au gates that were functionalized with NHC-based ligands. Gold was selected as the gate material, as it is inert, biocompatible, and capable of withstanding harsh chemical cleaning processes. Successful NHC functionalization on Au surfaces was first confirmed and verified. To illustrate the potential of NHC-modified OECTs in biosensing, biotin molecules were attached to the NHC-Au gate via click chemistry, allowing selective detection of streptavidin (SA). The biotin-SA pair, chosen based on the high binding affinity, serves as a proof-of-concept to demonstrate the potential of using OECTs combined with NHC ligands for affinity-based biosensors. Long-term stability of NHC-modified Au electrode and the printed OECTs was shown for up to 24 months after functionalization. This work presents an alternative functionalization group to enhance the sensing capability of OECT-based biosensors and demonstrates the development of a generalized biosensor platform with exceptional stability and reliability, making it readily adaptable to a variety of biomolecule detection methods.

2 Materials and methods

2.1 Au gate electrode and OECT fabrication

The Au gate electrodes and OECTs were printed using Optomec Aerosol Jet 5X 3D printer on flexible polyimide substrates based on the process reported previously (Fan et al., 2023). The Au gate, source and drain electrodes of OECT were printed using gold nanoparticle (Au NP) ink (UT Dots, Inc.) and deposited using

the ultrasonic atomizer (UA). The printed Au traces were annealed at 280°C for 1 h on a hotplate. The channel of OECT was printed with UA using poly (3,4-ethylenedioxythiophene) polystyrene sulfonate (PEDOT:PSS) mixture composed of 94% Heraeus Clevios™ PH 1000, 5% ethylene glycol (EG), 0.1% dodecylbenzenesulfonic acid solution (DBSA) (70 wt% in isopropanol), and 1 wt% (3-glycidyloxypropyl) trimethoxysilane (GOPS) (≥98%) and annealed in an oven at 130°C for 20 min. Finally, a layer of UV-curable polydimethylsiloxane (PDMS) (Shin-Etsu Chemical Co., Ltd.) diluted with hexanes with a volume ratio of 3:1 was deposited by the pneumatic atomizer (PA) to protect the metal traces from shorting with the liquid electrolyte. The PDMS insulating layer was cured with UV on-the-fly while printing and then annealed at 130°C for 30 min.

2.2 NHC ligand synthesis

The NHC ligand synthesis was adopted from Johnson et al. (Johnson and Gimeno, 2017) and carried out under a nitrogen environment using the Schlenk technique. Imidazole (500 mg) was dissolved in 50 mL of anhydrous acetonitrile. 2.42 mL of 3-bromo-1-(trimethylsilyl)-1-propyne was added to the imidazole solution. The resulting mixture was heated to 80°C and stirred for 24 h. After the mixture was cooled to room temperature, the solvent was removed under vacuum to leave a brown solid that was then washed with diethyl ether multiple times to remove impurities and unreacted reagents to yield the NHC ligand as a light brown solid. The material composition was verified by nuclear magnetic resonance (NMR) spectroscopy with spectral data (Supplementary Figure S1) similar to those reported in previous literature (Johnson and Gimeno, 2017). ^{1}H-NMR (600 MHz, DMSO-d_6), δ (ppm): 9.18 (s, ^{1}H, NCHN), 7.86 (s, ^{1}H, NCH = CHN), 7.7 (s, ^{1}H, NCH = CHN), 5.3 (d, J = 5.6 Hz, ^{4}H, 2xCH_2 = CH), 0.05 (m, J = 13.4 Hz, 2xSi-$(CH_3)_3$). ^{13}C-NMR (150 MHz, DMSO-d_6) δ (ppm): 136.4 (NCHN), 123.2, 119.7 (NCH = CHN), 98, 93 (C≡C-CH_2), 79.9 (CH_2-C≡C), 40.2, 39.7 (N-CH_2-C≡CH) (masked by solvent).

2.3 Alkyne-NHC deposition on Au

Before functionalization, the printed Au gate electrodes were cleaned thoroughly with acetone, isopropanol, ethanol, and deionized (DI) water, dried under nitrogen, and kept under vacuum. To ensure the Au electrodes were in place during the reaction, they were fixed to the sidewall of a round bottom flask using double-sided Kapton tapes. The SAM was formed by immersing the Au electrode in a heated solution of the synthesized NHC ligand and potassium-*tert*-butoxide dissolved in anhydrous acetonitrile under a nitrogen environment for 48 h. The functionalized electrodes were cleaned with acetonitrile and DMSO and dried under vacuum. Deprotection of the terminal alkyne groups was carried out by immersing the NHC functionalized Au electrodes in a solution of K_2CO_3 in methanol/tetrahydrofuran (THF) (volume ratio of 1:1) for 30 min. The resulting alkyne-NHC Au electrodes were cleaned with methanol and dried under nitrogen.

2.4 Copper (I)-catalyzed alkyne-azide cycloaddition

Copper (I)-catalyzed alkyne-azide cycloaddition (CuAAC) was used to attach fluorescein and biotin molecules to the alkyne-NHC functionalized Au electrodes. The click chemistry was performed under ambient conditions based on procedures reported elsewhere (Presolski et al., 2011; Goodge and Frey, 2020).

To verify the click chemistry reaction, azide-fluorescein was used to modify the Au electrode. The fluorescence can then be used for imaging after surface functionalization. The reaction was carried out by mixing azide-fluorescein (1 equiv.), copper (II) sulfate pentahydrate ($Cu_2SO_4{\cdot}5H_2O$) (2 equiv.), and L-ascorbic acid (L-AA) (10 equiv.) in 20 mL ultrapure water under dark conditions for 24 h. The electrodes were then rinsed multiple times with DI water and soaked in DI water for 1 h to remove unreacted molecules and reaction by-products. The functionalized electrodes were dried with nitrogen and kept in the dark under vacuum before taking fluorescence images.

The immobilization of biotin was carried out by immersing the NHC functionalized Au electrodes in a solution of 1 equiv. azide-PEG_7-biotin, 2 equiv. $Cu_2SO_4{\cdot}5H_2O$, and 10 equiv. L-AA in 20 mL ultrapure H_2O for 24 h. The electrodes were then rinsed with DI water, soaked in DI water for 1 h to remove the unreacted molecules, and dried under nitrogen. The biotin functionalized electrodes were kept in a sample desiccator before the measurements.

2.5 Characterization of functionalized Au electrodes

2.5.1 X-ray photoelectron spectroscopy (XPS)

XPS measurements were performed using a Kratos Axis (Ultra) spectrometer with monochromatized Al Kα (hυ = 1,486.71 eV) and calibrated using the binding energy (84.0 eV) of Au 4f7/2 reference to Fermi level. The measurements were carried out in an analysis chamber pressure lower than 5×10^{-10} Torr. A hemispherical electron-energy analyzer with pass energy of 20 eV was used to collect core-level spectra, while survey spectrum within binding energies ranging from 0 to 1,100 eV was collected at analyzer pass energy of 160 eV. Charge effects were corrected by using C1s peak at 284.8 eV. A Shirley background was applied to subtract the inelastic background of core-level peaks. Non-linear optimization using the Marquardt Algorithm (CasaXPS) was used to determine the peak model parameters, such as positions, widths, and intensities. The peak fitting was based on a product of Gaussian and Lorentzian functions. Composition ratios were calculated from the survey spectra using the N1s and C1s peaks and the sensitivity factors provided by the database. CasaXPS was used for component analysis to fit the high-resolution spectra of C1s and N1s.

2.5.2 Fluorescence imaging

The Au electrodes modified with fluorescein and biotin via click chemistry were imaged using a ChemiDoc™ MP Gel Imaging System with the samples covered in 1xPBS solution.

2.5.3 Electrochemical measurements

The electrochemical measurements were conducted using a Gamry Reference 600+ potentiostat. All the measurements were performed at room temperature using a standard three-electrode configuration where the modified printed Au electrode acted as the working electrode, Pt wire acted as the counter electrode, and an Ag/AgCl (in saturated KCl) reference electrode was used. All the measurements were carried out in a 10 mL cell containing 5 mM $K_4Fe(CN)_6/K_3Fe(CN)_6$ aqueous solution with 100 mM KCl supporting electrolyte. The cyclic voltammetry measurements were collected by scanning between −0.2 and +0.7 V vs. Ag/AgCl with a scan rate of 50 mV/s for three cycles, and the third cycle was used for analysis. The EIS measurements were obtained at frequencies ranging from 0.01 Hz to 100 kHz with 5 mV AC amplitude and potential at 0.3 V vs. Ag/AgCl. Echem Analyst software was used to analyze the data.

2.6 Electrical characterization of OECTs with functionalized gate

All the electrical measurements of OECT were performed using a Keithley 2612B source measure unit and Signatone micropositioner probes controlled by LabView. 1xPBS was used as the electrolyte for all the measurements. The transfer characteristics were obtained by measuring the drain current (I_D) under a constant drain bias (V_D) of −0.2 V and sweeping the gate voltage (V_G) from −0.4 to 1.2 V. The operation voltage ranges were selected to balance the OECT performance and maintain electrochemical stability. The threshold voltage (V_T) was extracted from the transfer curve based on the linear extrapolation method (Doris et al., 2018). First, find the *x*-intercept (V_x) by extending the portion of the curve with maximum slope, and then add $V_D/2$ to V_S. Therefore, V_T can be calculated based on Equation 1:

$$V_T = V_x + \frac{V_D}{2} \quad (1)$$

Streptavidin (SA) and bovine serum albumin (BSA) proteins were dissolved in 1xPBS to 1 mg/mL solutions. For measuring the biotin-streptavidin binding, 50 µL of 1 mg/mL SA solution was placed onto the biotin-NHC-Au electrodes for 1 h, and the electrodes were thoroughly washed with PBS and DI water before measurements. To test the selectivity of biotin-NHC-Au electrodes, they were immersed in 50 µL 1 mg/mL BSA solution, thoroughly washed with PBS and DI water, and used for OECT measurements.

The sensitivity of analyte detection was calculated based on the device threshold voltage shifts (ΔV_T) using Equation 2:

$$\Delta V_T = V_{T,after} - V_{T,before} \quad (2)$$

where $V_{T,before}$ and $V_{T,after}$ represent the device V_T measured before and after functionalization or analyte incubation, respectively.

3 Results and discussions

3.1 Printed Au electrode functionalization

The overall process flow of fabrication, functionalization, and measurement of OECT based biosensor with functionalized gates is illustrated in Figure 1A. The printed Au gate electrodes consisted of two 9 mm^2 squares connected by a 300 µm wide Au trace (Figures 1B, C). The size of the electrode working area was optimized before functionalization to ensure a low OECT operating voltage. As observed from Supplementary Table S1, the lowest gate voltage for the maximum transconductance (g_m) was obtained for an OECT with a gate size of 9 mm^2. Moreover, our previous study demonstrated that although g_m is mainly dependent on channel dimensions, larger gate sizes led to enhanced sensitivity. This increase is due to increased functionalization area, allowing more bioreceptors to attach (Fan et al., 2023). During functionalization, only one end of the electrode was immersed in the ligand solution to control the area of modification. The other Au pad served as an electrical connection to ensure low contact resistance for the electrochemical measurements. The NHC SAM deposition reaction schematic is shown in Figure 1D. The Au electrodes were immersed in the ligand solution to form tetramethylsilane (TMS) terminated alkyne functionalized NHC (TMS-alkyne-NHC) monolayer. Then, the TMS protection groups were removed, leaving alkyne-NHC groups on the printed Au electrode surface. NHC ligands were engineered with alkyne functional groups to facilitate biomolecule immobilization through well-studied click chemistry.

XPS and electrochemical measurements were performed on the modified Au electrodes to verify the alkyne-NHC deposition. XPS measurements were conducted on the blank Au film and alkyne-NHC Au samples. As the blank Au was printed and annealed under ambient conditions, it is possible to have environmental nitrogen and carbon contaminations. The survey scans of a blank Au and alkyne-NHC Au in Supplementary Figure S2 reveal that the nitrogen (N1s) composition in the blank Au sample is much lower than the alkyne-NHC Au sample. For the alkyne-NHC Au sample, the increased N1s composition confirms the surface modification. Figures 2A–D shows the comparison of high resolution XPS spectra for a blank Au and an alkyne-NHC Au film. The central peak of N1s spectrum for the alkyne-NHC Au film was detected at around 400.5 eV, which is 0.5 eV higher than the value measured for the blank Au film. Similarly, the C1s peak for the alkyne-NHC Au sample was centered at around 284.7 eV, which is 0.3 eV higher than the C1s peak observed for the blank Au film. These values are comparable to the literature values of 400.45 eV for N1s and 284.84 eV for C1s obtained by Sherman et al. (Sherman et al., 2021). NHC deposition on the printed Au electrodes was further verified with electrochemical measurements. CV and EIS were performed using the same printed Au electrode before and after NHC functionalization. For CV plots (Figure 2E), the anodic current peak decreased from 115.7 µA to 104.3 µA, and the peak separation increased from 104.8 mV to 117.7 mV after the alkyne-NHC functionalization. The Nyquist plots (Figure 2F) reveal a clear change in the electrode impedance (equivalent circuit and analysis are shown in Supplementary Figure S3) after NHC functionalization.

Additional verification of NHC deposition on the Au surface was confirmed by contact angle and attenuated total reflectance - Fourier transform infrared (ATR-FTIR) spectroscopy measurements. Contact angle measurements were performed on Au-coated glass samples. The Au surface becomes more hydrophilic

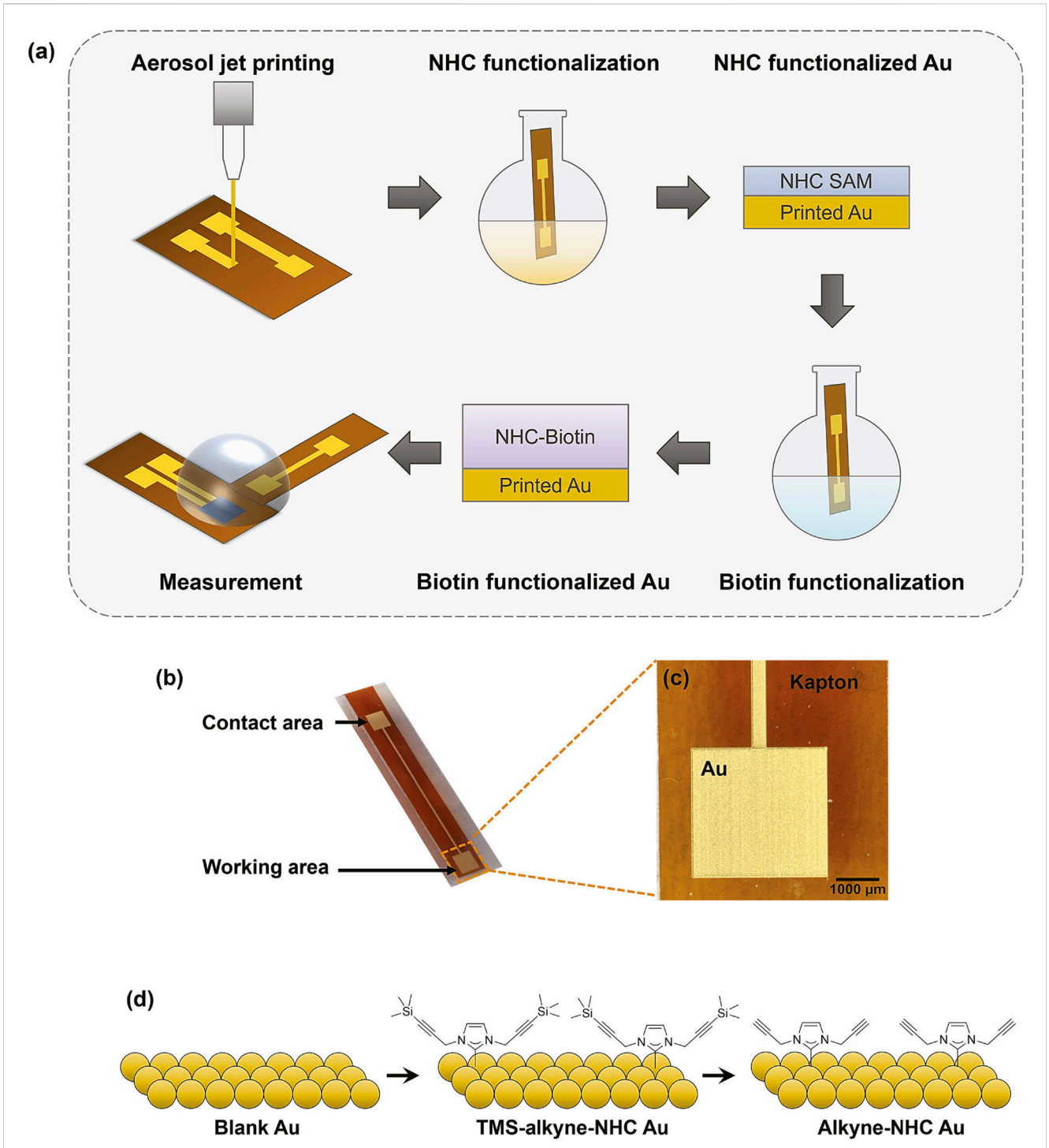

FIGURE 1
(A) Schematic illustration of the fabrication, functionalization, and measurement of OECT based biosensor. **(B)** Digital photo of a printed Au gate electrode on Kapton substrate. **(C)** Microscope image showing the zoom-in view of the printed Au electrode. **(D)** Reaction schematic of attaching NHC-alkyne to the Au surface.

after alkyne-NHC modification, decreasing from 87.00° to 42.22° (Supplementary Figure S4). Finally, characteristic peaks are observed in the IR spectrum of a TMS-alkyne-NHC modified printed Au electrode, as shown in Supplementary Figure S5. It should be noted that the measurements were conducted with electrodes from multiple functionalization batches and different functionalization areas. These results, therefore, confirm that alkyne-NHC functional groups were successfully deposited onto the printed Au electrode surface.

Copper (I)-catalyzed alkyne-azide cycloaddition (CuAAC) was adopted for attaching the biomolecules in this work, and the reaction schematics are shown in Figure 3. The click chemistry reaction was

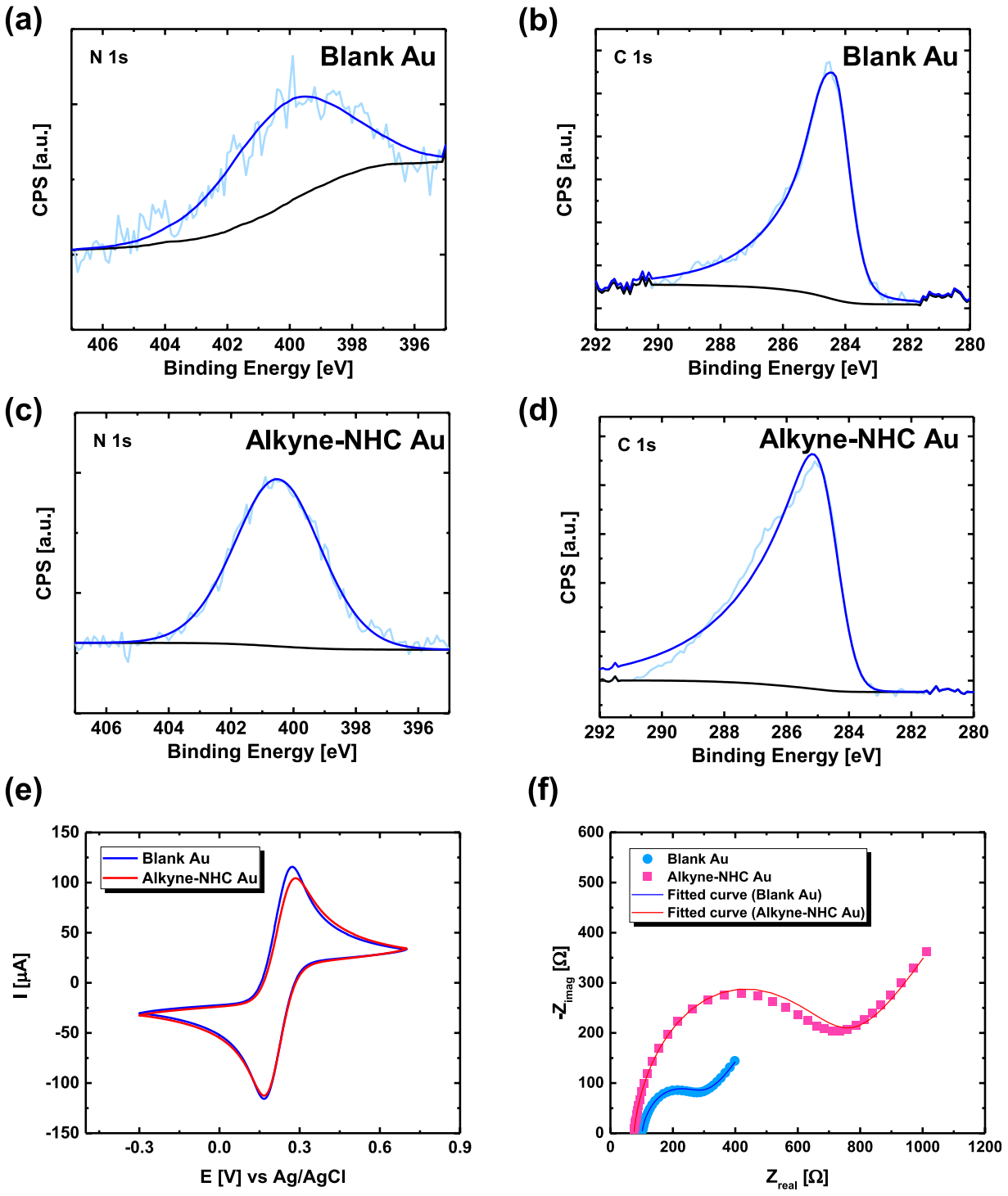

FIGURE 2
(A) High-resolution XPS spectra showing N1s region for a blank Au electrode with a peak centered at 400.0 eV and **(B)** C1s region for the blank Au electrode with a peak at 284.4 eV **(C)** XPS N1s and **(D)** C1s spectra for an alkyne-NHC Au sample with peaks at 400.5 eV and 284.7 eV, respectively. **(E)** CV and **(F)** EIS of a printed Au electrode before (blue) and after (red) alkyne-NHC deposition.

first performed using azide-fluorescein to verify the conditions. The reagents were added into a round bottom flask with 20 mL of ultrapure water, and the Au electrodes were immersed in the solution for 24 h under dark ambient conditions. The control experiment was performed by immersing a blank Au electrode and the alkyne-NHC functionalized Au electrodes in the same solution. From the fluorescence images (Figure 4A) captured for the Au electrodes, it could be clearly observed that fluorescein molecules only attached to the alkyne-NHC modified Au electrode as expected. No fluorescence was observed for the

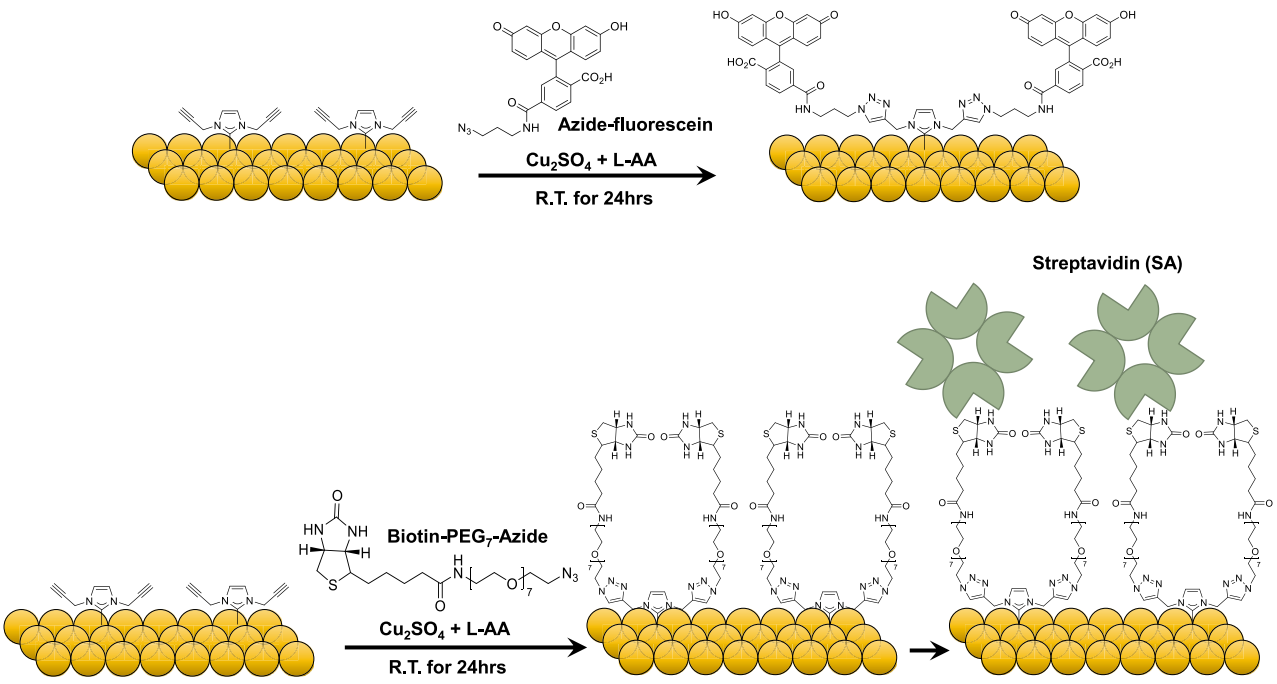

FIGURE 3
Reaction schematic of Copper (I)-catalyzed alkyne-azide cycloaddition (CuAAC) for attaching azide-fluorescein and azide-PEG$_7$-biotin.

control or the blank Au electrode. The surface modification was further confirmed with CV measurements. Figure 4B shows the electrochemical measurements of an alkyne-NHC Au electrode before and after attaching fluorescein. After functionalizing with fluorescein, the anodic peak current was reduced by 17.1 μA and the peak separation increased by 70.4 mV. Therefore, these results are evidence of the successful attachment of fluorescein molecules onto the Au electrode via the NHC linker and click chemistry.

The potential of using the alkyne-NHC Au electrodes for biosensor development was validated using the well-established biotin-streptavidin (biotin-SA) pair, which serves as a reference for new biosensor development in various studies (Guo et al., 2010; Voisin et al., 2014; Lowe et al., 2017; Molazemhosseini et al., 2021). Azide-PEG$_7$-biotin molecules were attached to the NHC-modified Au electrode via click chemistry. CV measurements were performed on the biotin-modified Au electrode before and after streptavidin binding. As shown in Figure 4C, the reduction in CV anodic peak amplitude and increase in the CV peak separation was an indication that the biotin molecules were bound to the alkyne-NHC Au surface.

3.2 Streptavidin (SA) detection using OECT

As a proof-of-concept, the functionalized Au electrodes were implemented as an external gate electrode for an OECT measurement configuration to characterize biotin-SA binding events. As shown in the microscopic image in Figure 5A, the OECT channel dimension was optimized to be L = 100 μm and W/L = 10, based on our previous work for high g_m (Rezaie et al., 2020; Fan et al., 2023). The typical output characteristics, transfer curve, and transconductance curve of a printed OECT are shown in Supplementary Figure S6. As shown in the experimental setup photo (Figure 5B), the functionalized Au electrode was placed next to an OECT on a clean gel box to ensure that they stayed in the same position with respect to each other during the measurement, and we added sufficient electrolyte to ensure both the channel and the modified area of the gate electrode were fully covered. By separating the functionalized gate electrode from the OECT, we were able to reuse the same OECT for multiple measurements and validate the gate functionalization across different devices. If a bioreceptor-analyte pair with a reversible interaction is selected, the NHC-functionalized gate electrode could also potentially be reused for multiple detection rounds.

The effects of functionalization were analyzed by comparing the transfer curves measured after each step of the modification using the same OECT device. Figure 5C shows that the transfer curve of the OECT shifted to a lower V_G by 247 mV after functionalizing the gate with biotin. After incubating the gate electrode in SA solution, an opposite shift of the transfer curve to a higher V_G by 177 mV was observed, which was a result of the biotin-SA binding reaction. The corresponding curves before normalization are shown in Supplementary Figure S7. The biotin attachment and SA binding to biotin led to interfacial potential profile change at the OECT gate/electrolyte, which altered the transfer characteristics. Consistent trends of transfer curve shifts were consistent for multiple electrodes and confirmed with multiple OECT devices.

To investigate the selectivity of SA detection with OECT, the biotin modified Au electrode was tested after incubating in bovine serum albumin (BSA) solution. BSA has been widely utilized as a blocking agent on sensor surfaces due to its high adsorption on various surfaces. Therefore, BSA was used to study the interference from non-specific surface adsorption and assess the sensor

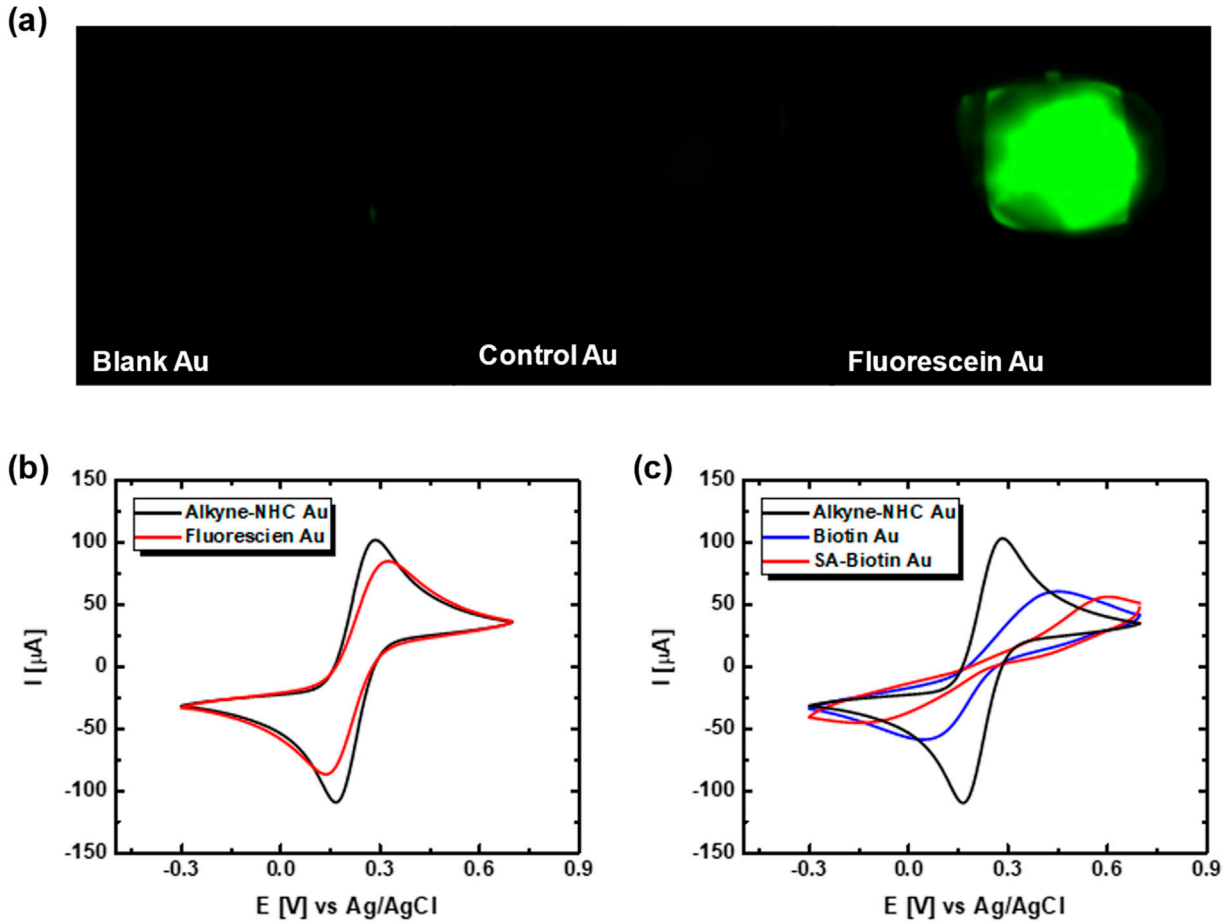

FIGURE 4
(A) Fluorescence image of an unfunctionalized printed Au electrode, a control Au electrode, and a fluorescein modified Au electrode. **(B)** CV of an alkyne-NHC Au electrode before (red) and after (green) fluorescein molecule attachment. **(C)** CV of an alkyne-NHC Au electrode before (black) and after (blue) biotin functionalization and after streptavidin (SA) binding (red).

selectivity. After BSA incubation, there was a small shift in the transfer curve to higher V_G by 33 mV (Figure 5D). This is likely due to the non-specific adsorption of a small amount of BSA molecules onto the electrode surface. The change after BSA incubation is significantly lower than the change observed after binding with SA. Therefore, the biotin functionalized gate electrodes have selectivity towards SA.

Change in the transfer characteristics is quantified by extracting the threshold voltage (V_T) from each measurement, and the change of V_T (ΔV_T) was calculated. As listed in Supplementary Table S2, although V_T value varies among devices, the V_T values for the same device extracted for three measurements under the same testing conditions have standard deviations (σ) less than 10 mV. The average σ for V_T acquired for 12 different OECTs was only 3 mV. This indicates that the printed OECTs exhibit excellent stability, and the V_T change is mainly due to functionalization and biomolecule binding. As shown in Figure 5E, the overall average ΔV_T of freshly prepared NHC-Au electrodes after biotin functionalization, SA binding, and BSA incubation are −267 ± 45 mV, 193 ± 64 mV, and 62 ± 41 mV, respectively. A larger average ΔV_T was obtained for SA than BSA, exhibiting a target-specific sensor response. The change due to non-specific binding is approximately 30% of the response due to SA binding. A higher standard deviation of the average ΔV_T after SA binding was observed, which is likely due to the variation in the actual units of SA protein bound to the functionalized surface. SA is a tetramer, and each subunit binds to one biotin molecule. One SA molecule can react with up to four biotin molecules, which could be the four neighboring molecules or at a nearby distance due to the PEG spacer arm length. Hence, some biotin molecules might be blocked from the reaction, leading to variations in the amount of SA bound to each electrode.

One of the major advantages is the robustness and outstanding stability of NHC functionalized surfaces. From our experiences, the TMS-alkyne-NHC-Au samples can be stored under ambient conditions for at least several months without deterioration. Exploiting this advantage, we were able to batch process four to six electrodes during NHC deposition and kept them for later use. The IR spectrum collected on biotin-functionalized Au electrode still had characteristic peaks for NHC after 20 months of storage in a sample desiccator at room temperature (Supplementary Figure S8). Moreover, we conducted the biotin functionalization and the

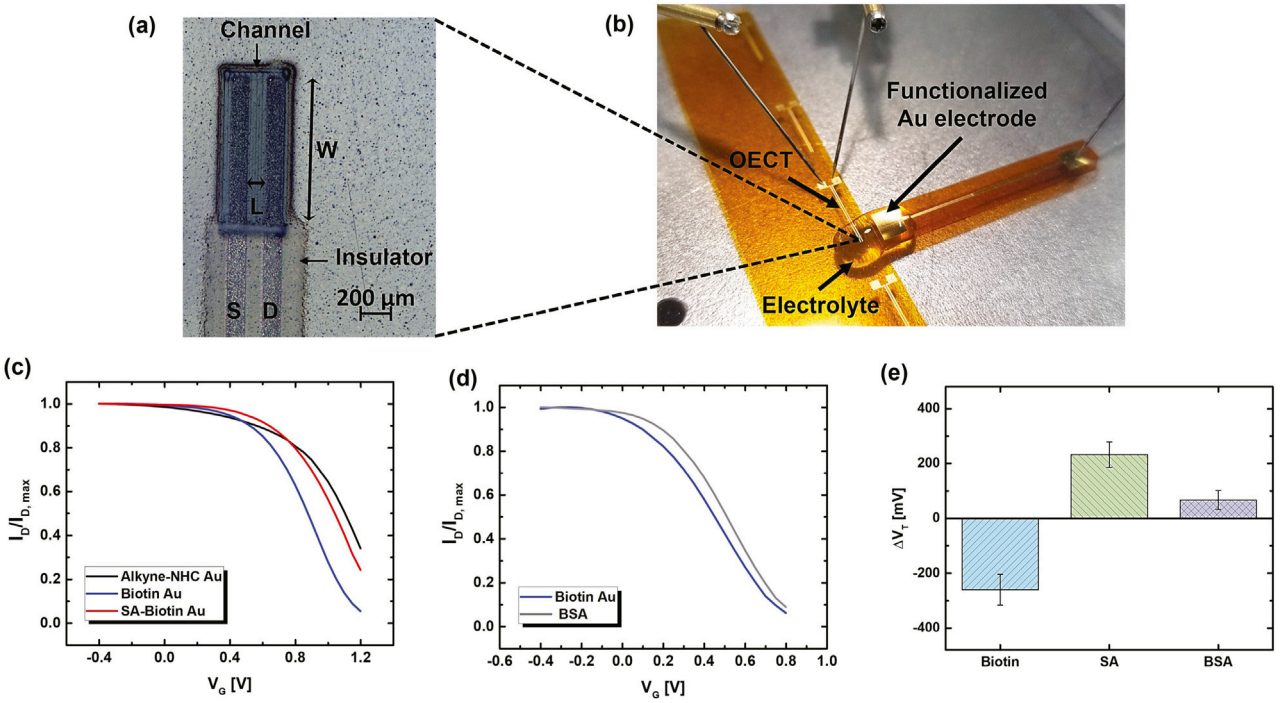

FIGURE 5
(A) Microscope image of a printed OECT. **(B)** Photograph of the OECT based biosensor measurement setup. **(C)** Normalized transfer curves (I_D-V_G) acquired using an alkyne-NHC Au gate electrode (black), after biotin attachment (blue), and after SA binding (red). The corresponding raw data plots are shown in Supplementary Material (Supplementary Figure S7A). **(D)** Normalized I_D-V_G for a biotin modified printed Au electrode before (blue) and after (grey) immersing in BSA solution, showing a small shift due to non-specific BSA binding. The corresponding raw data plots are shown in Supplementary Material (Supplementary Figure S7B). **(E)** The average change in the threshold voltage (ΔV_T) extracted from transfer curves of OECTs measured using freshly functionalized alkyne-NHC-Au electrodes after biotin functionalization, SA binding, and BSA incubation for selectivity test. The BSA-SA binding measurements were repeated on two different electrodes each with three OECT devices to confirm repeatability. The BSA selectivity test was performed on two electrodes each measured with one OECT. Error bars represent standard deviation.

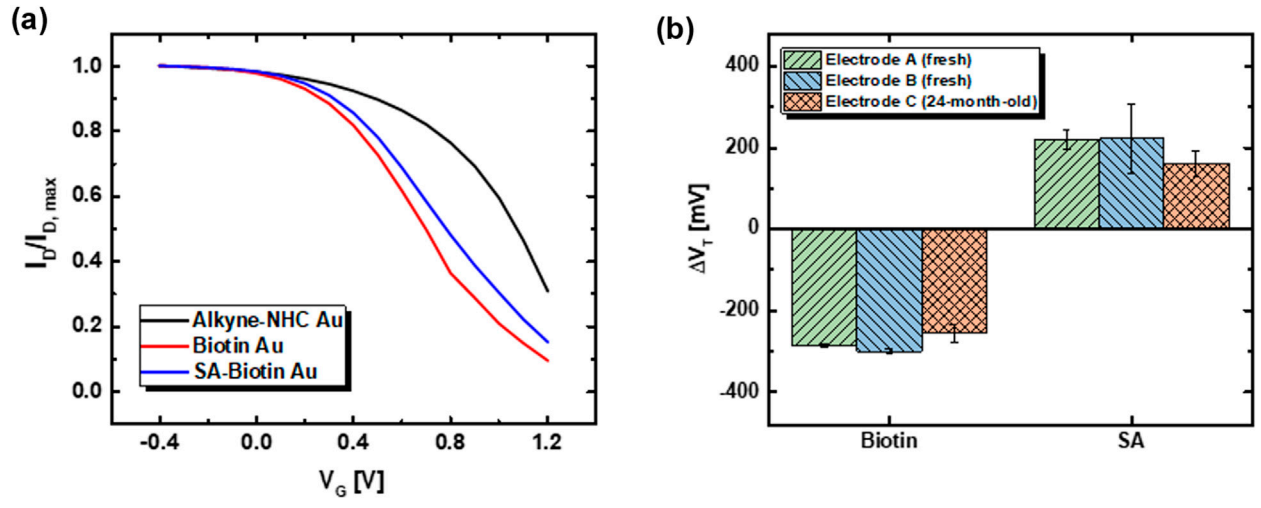

FIGURE 6
(A) Normalized I_D-V_G for an alkyne-NHC-Au electrode after 24 months of storage in sample desiccator (black), and subsequently measured after biotin functionalization (red) and SA binding (blue). The transfer curve shift followed the same trend as that observed for the freshly functionalized electrodes. **(B)** Average ΔV_T extracted from measurements acquired using the two freshly functionalized electrodes and one 24-month-old alkyne-NHC-Au electrode after biotin functionalization and SA binding. Each freshly prepared electrode was measured with three different OECTs to obtain the average. For the 24-month old electrode, three measurements were conducted using the same 24-month-old OECT. Error bars represent standard deviation.

detection of SA binding using an alkyne-NHC-Au electrode after storing it in a sample desiccator for 24 months at room temperature. Our printed OECT demonstrated remarkable long-term stability, with minimal electrical performance deterioration over 24 months of storage period under ambient conditions at room temperature. The electrical characteristics acquired within a few days after the OECT fabrication and after a 24-month storage period are shown in Supplementary Figure S9. To the best of our knowledge, this is the first time that such long-term stability of OECT has been reported. The same measurements were performed using the 24-month-old gate electrode and OECT device. As shown in Figure 6A, the same trend of transfer curve shift was observed for the 24-month-old alkyne-NHC-Au electrode as the freshly prepared ones.

Average ΔV_T for individual electrodes are plotted in Figure 6B to compare the performances of biosensing with their values listed in Supplementary Table S3. For the alkyne-NHC-Au electrode stored 24 months after functionalization, the average ΔV_T after biotin functionalization and SA binding are −255 ± 20 mV and 161 ± 30 mV, respectively. These values are comparable to those for freshly functionalized NHC electrodes. Based on the standard deviation of the ΔV_T after biotin functionalization, the limit of detection (LOD) of this functionalized electrode, calculated based on 3-sigma (3σ) method, is 60 mV. The average ΔV_T after SA binding is approximately 2.6 times the value of 3σ. This indicates that the change we observed was well above the LOD of the electrode, which confirms its capability of biosensing even after 24 months of storage. Our observation indicates that NHCs have outstanding long-term stability for surface functionalization. The exceptional stable performance of printed OECTs helps to eliminate the potential detection error arising from device deterioration and contributes towards more reliable biosensing performance. However, the stability of the biorecognition element and the linkage between the biomolecule and the NHC functional group is another crucial aspect affecting the overall shelf-life of the biosensor. Further research is required to gain a deeper understanding of these correlations.

The stability of NHC surface ligands has been investigated in other studies under various conditions. The NHC functionalized Au nanoparticles remain stable for at least 21 days when suspended in various biological media, including buffers, cell culture media, and full-strength human serum (Sherman et al., 2022). As demonstrated by Crudden et al., the NHC functionalized Au electrode showed remarkable stability under repeat electrochemical measurements (150 cycles) with no detectable change in the current density, whereas Au electrode functionalized with dodecanethiol showed a 600% increase due to SAM film defects (Crudden et al., 2014). Similarly, Mayall et al. observed a 10 times higher response and a longer shelf life for the NHC-based electrochemical biosensor as compared to the thiol-based system (Mayall et al., 2020). The bacteria biosensors based on NHC SAMs and toll-like receptor proteins exhibited no loss in their sensing ability over 4 weeks (Singh et al., 2021). Kim et al. demonstrated pathogen sensing in clinical samples using ultra-stable biosensors based on NHC-graphene nanotransistors with a side-gate design, and they designed NHC derivatives to enable highly stable covalent bonding with graphene (Kim et al., 2024). The remarkable stability of NHC modified Au surfaces creates new possibilities for employing various modification strategies to achieve desired surface functionalization. Thus, OECTs with NHC functionalized gates offer a promising approach to developing biosensing devices with long-term stability at room temperature.

4 Conclusion

In conclusion, we successfully demonstrated the functionalization of aerosol jet-printed Au electrodes with NHC for biosensing applications. The detection of streptavidin-biotin binding was achieved by incorporating the NHC-modified Au electrode as the gate for a printed OECT. The biotin functionalization and SA binding were observed as shifts in the OECT transfer curve due to interfacial potential profile change within the device. An average shift of −267 ± 45 mV was observed after biotin attachment. The biosensors exhibit selective responses towards SA, as expected, with ΔV_T of 193 ± 64 mV, which is about a factor of three compared to the ΔV_T for non-specific BSA binding (62 ± 41 mV). The alkyne-NHC-Au electrode retained its functionality after being stored for 24 months at room temperature, with ΔV_T of −255 ± 21 mV and 161 ± 30 mV for biotin functionalization and SA binding, respectively. These values are comparable with freshly prepared NHC-Au electrodes, indicating outstanding stability. Remarkably, the printed OECT retained its full electrical performance after 24 months stored under ambient conditions. Our findings highlight NHCs as a promising candidate for long-term stable surface functionalization, and the printed OECTs can act as an ultra-stable transducer for biosensing applications. In this work, we synthesized the alkyne-NHC ligand to obtain the desired functional groups for specific reactions. However, there are commercially available NHC products, which may offer more convenient surface functionalization depending on the experimental requirements. By isolating the gate functionalization process, the OECT device performance was well-preserved, and each device could be used for repeated measurements with different electrodes to eliminate the effects of device variation. Hence, this work presents a versatile platform for the development of ultra-stable biosensors via printing and surface engineering, which is ready to be implemented for customizable biosensing applications.

Data availability statement

The raw data supporting the conclusions of this article will be made available by the authors, without undue reservation.

Author contributions

JF: Data curation, Formal Analysis, Investigation, Methodology, Validation, Visualization, Writing–original draft. SK: Data curation, Investigation, Validation, Writing–review and editing. MG: Conceptualization, Data curation, Formal Analysis, Funding acquisition, Methodology, Project administration, Supervision, Visualization, Writing–review and editing.

Funding

The author(s) declare that financial support was received for the research, authorship, and/or publication of this article. The authors would like to acknowledge NSERC grant number 06096 and Alberta Innovates for financial support. We also thank NSERC for the PGS-D funding for JF(PGSD-534859–2019).

Conflict of interest

The authors declare that the research was conducted in the absence of any commercial or financial relationships that could be construed as a potential conflict of interest.

Publisher's note

All claims expressed in this article are solely those of the authors and do not necessarily represent those of their affiliated organizations, or those of the publisher, the editors and the reviewers. Any product that may be evaluated in this article, or claim that may be made by its manufacturer, is not guaranteed or endorsed by the publisher.

Supplementary material

The Supplementary Material for this article can be found online at: https://www.frontiersin.org/articles/10.3389/fsens.2024.1430958/full#supplementary-material

References

Ataman Sadık, D., Eksi-Kocak, H., Ertaş, G., Boyacı, İ. H., and Mutlu, M. (2018). Mixed-monolayer of N-hydroxysuccinimide-terminated cross-linker and short alkanethiol to improve the efficiency of biomolecule binding for biosensing. *Surf. Interface Analysis* 50 (9), 866–878. doi:10.1002/sia.6489

Cerquera-Montealegre, L., Gallego, D., and Baquero, E. A. (2024). Recent advances in the catalytic applications of NHC-early abundant metals (Mn, Co, Fe) complexes. *Adv. Organomet. Chem.*, 181–270. doi:10.1016/bs.adomc.2024.04.001

Chen, L., Wu, J., Yan, F., and Ju, H. (2021). A facile strategy for quantitative sensing of glycans on cell surface using organic electrochemical transistors. *Biosens. Bioelectron.* 175, 112878. doi:10.1016/j.bios.2020.112878

Crudden, C. M., Horton, J. H., Ebralidze, I. I., Zenkina, O. V., McLean, A. B., Drevniok, B., et al. (2014). Ultra stable self-assembled monolayers of N-heterocyclic carbenes on gold. *Nat. Chem.* 6 (5), 409–414. doi:10.1038/nchem.1891

Doris, S. E., Pierre, A., and Street, R. A. (2018). Dynamic and tunable threshold voltage in organic electrochemical transistors. *Adv. Mater* 30 (15), e1706757. doi:10.1002/adma.201706757

Fan, J., Forero Pico, A. A., and Gupta, M. (2021). A functionalization study of aerosol jet printed organic electrochemical transistors (OECTs) for glucose detection. *Mater. Adv.* 2 (22), 7445–7455. doi:10.1039/d1ma00479d

Fan, J., Koh, A.-P., Wu, C.-S., Su, M.-D., and So, C.-W. (2024). Carbon dioxide capture and functionalization by bis (N-heterocyclic carbene)-borylene complexes. *Nat. Commun.* 15 (1), 3052. doi:10.1038/s41467-024-47381-7

Fan, J., Parr, S., Kang, S., and Gupta, M. (2023). Point-of-care (POC) SARS-CoV-2 antigen detection using functionalized aerosol jet-printed organic electrochemical transistors (OECTs). *Nanoscale* 15 (11), 5476–5485. doi:10.1039/d2nr06485e

Gentili, D., D'Angelo, P., Militano, F., Mazzei, R., Poerio, T., Brucale, M., et al. (2018). Integration of organic electrochemical transistors and immuno-affinity membranes for label-free detection of interleukin-6 in the physiological concentration range through antibody-antigen recognition. *J. Mater Chem. B* 6 (33), 5400–5406. doi:10.1039/c8tb01697f

Goodge, K., and Frey, M. (2020). Biotin-conjugated cellulose nanofibers prepared via copper-catalyzed alkyne-azide cycloaddition (CuAAC) "click" chemistry. *Nanomater. (Basel)* 10 (6), 1172. doi:10.3390/nano10061172

Guo, K., Wustoni, S., Koklu, A., Diaz-Galicia, E., Moser, M., Hama, A., et al. (2021). Rapid single-molecule detection of COVID-19 and MERS antigens via nanobody-functionalized organic electrochemical transistors. *Nat. Biomed. Eng.* 5 (7), 666–677. doi:10.1038/s41551-021-00734-9

Guo, Y., Ye, J. Y., Divin, C., Huang, B., Thomas, T. P., Baker, J. R., Jr., et al. (2010). Real-time biomolecular binding detection using a sensitive photonic crystal biosensor. *Anal. Chem.* 82 (12), 5211–5218. doi:10.1021/ac100576y

Hopkinson, M. N., Richter, C., Schedler, M., and Glorius, F. (2014). An overview of N-heterocyclic carbenes. *Nature* 510 (7506), 485–496. doi:10.1038/nature13384

Jadzinsky, P. D., Calero, G., Ackerson, C. J., Bushnell, D. A., and Kornberg, R. D. (2007). Structure of a thiol monolayer-protected gold nanoparticle at 1.1 A resolution. *science* 318 (5849), 430–433. doi:10.1126/science.1148624

Johnson, A., and Gimeno, M. C. (2017). Synthesis of propargyl-functionalized NHC gold complexes. *Organometallics* 36 (7), 1278–1286. doi:10.1021/acs.organomet.7b00012

Kang, S., Byeon, S. E., and Yoon, H. J. (2021). N carbene anchors in electronics applications. *Bull. Korean Chem. Soc.* 42 (5), 712–723. doi:10.1002/bkcs.12261

Kaur, G., Thimes, R. L., Camden, J. P., and Jenkins, D. M. (2022). Fundamentals and applications of N-heterocyclic carbene functionalized gold surfaces and nanoparticles. *Chem. Commun. (Camb)* 58 (95), 13188–13197. doi:10.1039/d2cc05183d

Kim, K. H., Seo, S. E., Park, S. J., Kim, J., Park, C. S., Le, T. H., et al. (2024). N-Heterocyclic carbene–graphene nanotransistor based on covalent bond for ultrastable biosensors. *Adv. Funct. Mater.* 34, 2310377. doi:10.1002/adfm.202310377

Lee, M.-T., Hsueh, C.-C., Freund, M. S., and Ferguson, G. S. (1998). Air oxidation of self-assembled monolayers on polycrystalline gold: the role of the gold substrate. *Langmuir* 14 (22), 6419–6423. doi:10.1021/la980724c

Li, Z., Munro, K., Ebralize, I. I., Narouz, M. R., Padmos, J. D., Hao, H., et al. (2017). N-heterocyclic carbene self-assembled monolayers on gold as surface plasmon resonance biosensors. *Langmuir* 33 (49), 13936–13944. doi:10.1021/acs.langmuir.7b03280

Li, Z., Munro, K., Narouz, M. R., Lau, A., Hao, H., Crudden, C. M., et al. (2018). Self-assembled N-heterocyclic carbene-based carboxymethylated dextran monolayers on gold as a tunable platform for designing affinity-capture biosensor surfaces. *ACS Appl. Mater. and interfaces* 10 (21), 17560–17570. doi:10.1021/acsami.8b02595

Liao, J., Si, H., Zhang, X., and Lin, S. (2019). Functional sensing interfaces of PEDOT: PSS organic electrochemical transistors for chemical and biological sensors: a mini review. *Sensors (Basel)* 19 (2), 218. doi:10.3390/s19020218

Liebana, S., and Drago, G. A. (2016). Bioconjugation and stabilisation of biomolecules in biosensors. *Essays Biochem.* 60 (1), 59–68. doi:10.1042/EBC20150007

Lim, C. Y., Owens, N. A., Wampler, R. D., Ying, Y., Granger, J. H., Porter, M. D., et al. (2014). Succinimidyl ester surface chemistry: implications of the competition between aminolysis and hydrolysis on covalent protein immobilization. *Langmuir* 30 (43), 12868–12878. doi:10.1021/la503439g

Liu, H., Yang, A., Song, J., Wang, N., Lam, P., Li, Y., et al. (2021). Ultrafast, sensitive, and portable detection of COVID-19 IgG using flexible organic electrochemical transistors. *Sci. Adv.* 7 (38), eabg8387. doi:10.1126/sciadv.abg8387

Lowe, B. M., Sun, K., Zeimpekis, I., Skylaris, C.-K., and Green, N. G. (2017). Field-effect sensors–from pH sensing to biosensing: sensitivity enhancement using streptavidin–biotin as a model system. *Analyst* 142 (22), 4173–4200. doi:10.1039/c7an00455a

Mayall, R. M., Smith, C. A., Hyla, A. S., Lee, D. S., Crudden, C. M., and Birss, V. I. (2020). Ultrasensitive and label-free detection of the measles virus using an N-heterocyclic carbene-based electrochemical biosensor. *ACS Sens.* 5 (9), 2747–2752. doi:10.1021/acssensors.0c01250

Molazemhosseini, A., Viola, F. A., Berger, F. J., Zorn, N. F., Zaumseil, J., and Caironi, M. (2021). A rapidly stabilizing water-gated field-effect transistor based on printed single-walled carbon nanotubes for biosensing applications. *ACS Appl. Electron Mater* 3 (7), 3106–3113. doi:10.1021/acsaelm.1c00332

Nuzzo, R. G., Zegarski, B. R., and Dubois, L. H. (1987). Fundamental studies of the chemisorption of organosulfur compounds on gold (111). Implications for molecular self-assembly on gold surfaces. *J. Am. Chem. Soc.* 109 (3), 733–740. doi:10.1021/ja00237a017

Presolski, S. I., Hong, V. P., and Finn, M. G. (2011). Copper-catalyzed azide-alkyne click chemistry for bioconjugation. *Curr. Protoc. Chem. Biol.* 3 (4), 153–162. doi:10.1002/9780470559277.ch110148

Qiao, X., Gou, X.-X., Li, Y., Li, J.-L., Yue, T., Sheng, Q., et al. (2023). Poly (N-heterocyclic carbene)-protected water-soluble gold nanoparticles with tunable functions for biosensing applications. *ACS Appl. Nano Mater.* 6 (3), 2218–2227. doi:10.1021/acsanm.2c05511

Rezaie, S. S., Gudi, D., Fan, J., and Gupta, M. (2020). Geometrical optimization of organic electrochemical transistor for high transconductance. *ECS J. Solid State Sci. Technol.* 9 (8), 081003. doi:10.1149/2162-8777/abb796

Schoenfisch, M. H., and Pemberton, J. E. (1998). Air stability of alkanethiol self-assembled monolayers on silver and gold surfaces. *J. Am. Chem. Soc.* 120 (18), 4502–4513. doi:10.1021/ja974301t

Shen, H., Abtahi, A., Lussem, B. R., Boudouris, B. W., and Mei, J. (2021). Device engineering in organic electrochemical transistors toward multifunctional applications. *ACS Appl. Electron. Mater.* 3, 2434–2448. doi:10.1021/acsaelm.1c00312

Sherman, L. M., Finley, M. D., Borsari, R. K., Schuster-Little, N., Strausser, S. L., Whelan, R. J., et al. (2022). N-heterocyclic carbene ligand stability on gold nanoparticles in biological media. *ACS Omega* 7 (1), 1444–1451. doi:10.1021/acsomega.1c06168

Sherman, L. M., Strausser, S. L., Borsari, R. K., Jenkins, D. M., and Camden, J. P. (2021). Imidazolinium N-heterocyclic carbene ligands for enhanced stability on gold surfaces. *Langmuir* 37 (19), 5864–5871. doi:10.1021/acs.langmuir.1c00314

Singh, I., Lee, D. S., Huang, S., Bhattacharjee, H., Xu, W., McLeod, J. F., et al. (2021). N-Heterocyclic carbenes meet toll-like receptors. *Chem. Commun. (Camb)* 57 (68), 8421–8424. doi:10.1039/d1cc03030b

Sophocleous, M., Contat-Rodrigo, L., García-Breijo, E., and Georgiou, J. (2020). Organic electrochemical transistors as an emerging platform for bio-sensing applications: a review. *IEEE Sensors J.* 21 (4), 3977–4006. doi:10.1109/jsen.2020.3033283

Srisombat, L., Jamison, A. C., and Lee, T. R. (2011). Stability: a key issue for self-assembled monolayers on gold as thin-film coatings and nanoparticle protectants. *Colloids Surfaces A Physicochem. Eng. Aspects* 390 (1-3), 1–19. doi:10.1016/j.colsurfa.2011.09.020

Stiernet, P., Pang, B., Taton, D., and Yuan, J. (2023). The promise of N-heterocyclic carbenes to capture and valorize carbon dioxide. *Sustain. Chem. Clim. Action* 2, 100018. doi:10.1016/j.scca.2023.100018

Strakosas, X., Sessolo, M., Hama, A., Rivnay, J., Stavrinidou, E., Malliaras, G. G., et al. (2014). A facile biofunctionalisation route for solution processable conducting polymer devices. *J. Mater Chem. B* 2 (17), 2537–2545. doi:10.1039/c3tb21491e

Voisin, V., Pilate, J., Damman, P., Megret, P., and Caucheteur, C. (2014). Highly sensitive detection of molecular interactions with plasmonic optical fiber grating sensors. *Biosens. Bioelectron.* 51, 249–254. doi:10.1016/j.bios.2013.07.030

Wang, N., Yang, A., Fu, Y., Li, Y., and Yan, F. (2019). Functionalized organic thin film transistors for biosensing. *Acc. Chem. Res.* 52 (2), 277–287. doi:10.1021/acs.accounts.8b00448

Welch, N. G., Scoble, J. A., Muir, B. W., and Pigram, P. J. (2017). Orientation and characterization of immobilized antibodies for improved immunoassays (Review). *Biointerphases* 12 (2), 02D301. doi:10.1116/1.4978435

Willey, T. M., Vance, A. L., Van Buuren, T., Bostedt, C., Terminello, L., and Fadley, C. (2005). Rapid degradation of alkanethiol-based self-assembled monolayers on gold in ambient laboratory conditions. *Surf. Sci.* 576 (1-3), 188–196. doi:10.1016/j.susc.2004.12.022

Zhang, L., Mazouzi, Y., Salmain, M., Liedberg, B., and Boujday, S. (2020). Antibody-gold nanoparticle bioconjugates for biosensors: synthesis, characterization and selected applications. *Biosens. Bioelectron.* 165, 112370. doi:10.1016/j.bios.2020.112370

Zhang, Y.-F., Li, X., Zhang, H., Wang, X.-Q., Sun, L.-Y., Duan, X.-L., et al. (2023). Gold (I) N-heterocyclic carbene complexes with tunable electronic properties for sensitive colorimetric detection of glutathione. *Mater. Chem. Front.* 7, 2880–2888. doi:10.1039/d3qm00167a

Zhukhovitskiy, A. V., Mavros, M. G., Van Voorhis, T., and Johnson, J. A. (2013). Addressable carbene anchors for gold surfaces. *J. Am. Chem. Soc.* 135 (20), 7418–7421. doi:10.1021/ja401965d